PHOTONICS Research

Ultrafast optical modulation of the fluorescence from a single-photon emitter in silicon carbide

Mengting He,[1] Yujing Cao,[1] Junjie Lin,[1] Zhiping Ju,[2,3] Botao Wu,[1] and E Wu[1,4,5,6,*]

[1]State Key Laboratory of Precision Spectroscopy, East China Normal University, Shanghai 200241, China
[2]Photon Technology (Zhejiang) Co., Ltd., Jiaxing 314100, China
[3]National Key Laboratory of Materials for Integrated Circuits, Shanghai Institute of Microsystem and Information Technology, Chinese Academy of Sciences, Shanghai 200000, China
[4]Department of Physics and Shanghai Key Laboratory for Magnetic Resonance, East China Normal University, Shanghai 200241, China
[5]Chongqing Key Laboratory of Precision Optics, Chongqing Institute of East China Normal University, Chongqing 401120, China
[6]Collaborative Innovation Center of Extreme Optics, Shanxi University, Taiyuan 030006, China
*Corresponding author: ewu@phy.ecnu.edu.cn

Received 9 January 2024; revised 1 March 2024; accepted 2 March 2024; posted 4 March 2024 (Doc. ID 517734); published 1 May 2024

The quest for the room-temperature optical transistor based on nonlinearities in single atoms or molecules is attracting a lot of attention. In this work, a single-photon emitter in cubic silicon carbide is verified that can operate as an optical switch at room temperature under pulsed green laser illumination with a near-infrared pulsed laser as the control gate. We demonstrated an ultrafast and reversible optical modulation with a high photoluminescence intensity suppression ratio up to 97.9% and a response time as short as 287.9 ± 5.7 ps. The current development provides insights for high-precision and ultrafast optical switches, with possibilities for integration with emerging electronic installations to realize more intelligent photoelectric integrated devices.

https://doi.org/10.1364/PRJ.517734

1. INTRODUCTION

The photonic transistor, which is the photonic counterpart of the electronic transistor, has many useful applications in optical communication [1], computing [2], and quantum information processing [3]. The quest for the optical switching and amplification promotes the development of optical transistors based on nanoscale objects, such as nanotubes, molecules, or atoms [4–7]. In an optical transistor, the propagation of the optical "signal" field is controlled by an optical "gate" field via nonlinear optical interaction [5]. As far as the single-photon source is concerned, the propagation of the signal is controlled by the presence or absence of a single photon in the gate field [5]. The requisite single-photon nonlinearity is generally weak, which leads to a challenge in application. Future optical communication technologies will ultimately rely on single atoms or molecules that can control light at the single-photon level since they have a high intrinsic nonlinearity, enabling to make use of the quantum nature of light.

Very recently, the single nitrogen-vacancy (NV) center has been demonstrated to be an optical switch under non-resonant continuous-wave illumination at room temperature [8], mainly due to its long-term photostability at room temperature [9–11]. Simultaneously, stable and efficient light emission with well-defined properties is always the focus of research with single-photon emitters (SPEs) [12]. As a kind of wide bandgap semiconductor material with similar physical properties to diamond, silicon carbide (SiC) has recently been employed as an alternative material in scalable and integrated quantum photonics [13–15]. The color centers in SiC attracts more and more attention owing to their quantum properties related to single-photon emission and coherent spin state control [13,16,17]. The ultrafast visible light all-optical switching in 6H-SiC is investigated with the highest modulation depth reaching 27% [18]. Besides, as an exceptionally photostable and bright SPE with excellent performance, its properties have been explored in recent years [19–23].

In this paper, we demonstrate an ultrafast optical-modulation-based SPE in cubic silicon carbide (3C-SiC) crystal. An ultrashort green pulsed laser and a strong near-infrared (NIR) pulsed laser were focused simultaneously on a single-color center in 3C-SiC crystal. The former served as the photoluminescence (PL) excitation source, while the latter was used to induce PL suppression as a control gate. The fluorescence intensity suppression ratio reached 97.9% and the response time was as short as 287.9 ± 5.7 ps. Investigations revealed the presence of dark states in the energy level of the SPE that can be optically activated by the NIR laser. As an application of this PL suppression effect, the supper-resolution microscope image beyond the diffraction limit was obtained with spatial resolution of 96.4 nm by applying a similar strategy to the stimulated emission depletion (STED) microscopy.

2. MATERIALS AND METHODS

Using a confocal fluorescence scanning microscope system as shown in Fig. 1, the optical excitation and detection of the SPE were investigated. As displayed in Fig. 1, the laser source used here was a dual-output Yb-doped fiber laser with a repetition rate of 20 MHz and a pulse duration of 12.5 ps. Output1 was at 532 nm and used to excite the defects in the 3C-SiC sample. Output2 was at 1064 nm and used as the suppressing laser beam. Since the two pulsed laser beams were from the same laser system, additional synchronization was not necessary. Both laser beams were forced to be linearly polarized by the two Glan prisms (GP1 and GP2) and the polarization directions could be adjusted by the half-waveplates (HWP1 and HWP2). A compact motorized translation stage (KMTS25E/M, Thorlabs) was used to vary the delay time Δt between the green and the NIR pulses. The green beam was focused on a piece of SiC crystal by an oil-immersion microscope objective (×100, N.A. = 1.40, oil immersion, Olympus UPlanSApo, Obj). The sample crystal was thermally annealed in the air at 800°C for 10 min. Collected by the same objective lens, the PL from the sample was spatially filtered by a telescope with a 30 μm pinhole and guided to the detection channel. The PL signal was then either detected by a silicon avalanche-photodiode-based single-photon counting detector (APD, Perkin Elmer, SPCM-AQR-14) or steered with a flip mirror (FM) to a spectrograph (ANDOR, 500i) for spectral analysis. Two detectors and a time-correlated single-photon counter (TCSPC) composed a Hanbury-Brown and Twiss setup to measure the time-correlation properties of the SPE and identify the unity of the optically active point defects. The NIR beam was aligned to overlap the green beam by the dichroic mirrors (DM1, DM2). The PL spectrum that could be detected covered from 580 to 960 nm due to the cutting edge of the DMs.

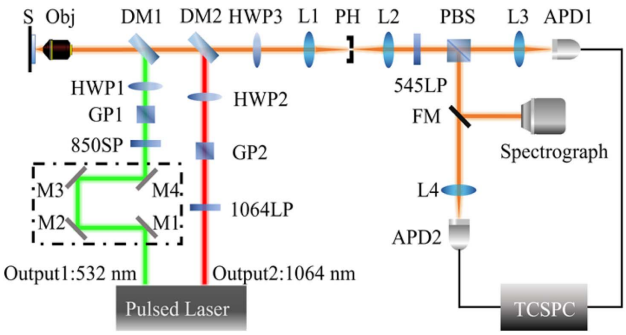

Fig. 1. Experimental setup. M1–4: mirrors; 850SP: short-pass filter cutting off at 850 nm; GP1, 2: Glan prisms; HWP1–3: half-waveplates; DM1: dichroic mirror reflecting the laser of 532 nm and passing the fluorescence longer than 580 nm; DM2: dichroic mirror reflecting the laser of 1064 nm and passing the fluorescence shorter than 980 nm; 1064LP: long-pass filter cutting off at 1064 nm; Obj: microscope objective lens; S: sample; L1–4: focusing lenses; PH: pinhole; 545LP: long-pass filter cutting off at 545 nm; PBS: polarized beam splitter; FM: flip mirror; APD1, 2: Si-avalanche photodiode single-photon detectors; TCSPC: time-correlated single-photon counter.

3. RESULTS AND DISCUSSION

A. Effect of NIR Laser Illumination

The 3C-SiC bulk crystal sample containing color centers was placed on the piezoelectric ceramics transducer. The PL signal from the emitters was recorded under the pulsed green laser excitation while scanning. Figure 2(a) displays a 2 μm × 2 μm confocal PL scanning image of the sample in $x \times y$ dimension, where a bright fluorescent spot can be observed. The room-temperature PL spectrum of this emitter under green laser excitation was obtained as shown in Fig. 2(b). According to the similar PL spectrum and lifetime reported in Ref. [24], we believe that the defects we studied here are oxidation-related defects in SiC resulting from annealing in an oxygen atmosphere [25]. The inset of Fig. 2(b) verifies the single-photon source nature of the color center by the photon anti-correlation with $g^2(0) = 0.11$. Most of the fluorescent points in the sample showed similar spectra and contained only one emitter generally.

The polarization properties can provide a demonstration of the electric dipole orientation of SPE. The excitation polarization direction of the green laser was tuned by rotating HWP1 and the total PL intensity was recorded as shown by the green dots in Fig. 2(c). The linear polarization contrast V up to 93.1% was obtained by fitting the experimental data according to

$$I = I_0(1 + V \cos \Delta\varphi). \quad (1)$$

Then, the emission polarization was studied by rotating HWP3 while fixing the green laser polarization direction at 90° for the maximum PL intensity. The PL intensity was recorded by APD1 behind the PBS. As shown by blue circles in Fig. 2(c), the PL intensity varied from 2 to 59 kilo-counts per second (kcps). The polarization contrast V of the emission was

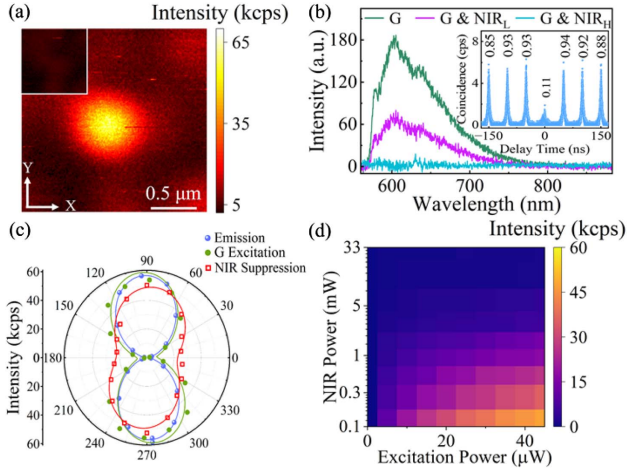

Fig. 2. (a) PL scan image in $x \times y$ dimension of the SPE when excited by the green laser. Inset: suppressed PL scan image of the SPE in the same region by adding the NIR laser. Note that the two images share the same intensity color bar. (b) PL spectra of the SPE pumped with only the green laser, with additional low-power NIR laser, and with high-power NIR laser. Inset: SPE PL photon-correlation. (c) Excitation polarization, emission polarization, and suppression polarization; (d) SPE PL intensity under simultaneous green and NIR excitations as a function of both green and NIR laser powers.

90.0% according to Eq. (1), illustrating that the SPE's PL was linearly polarized [26]. As the linear polarization contrasts of both the excitation and the emission are greater than 90%, we believe that the SPE had a single polarization, which is the characteristic of a single linearly polarized dipole transition. Additionally, the deviation between the measured emission and excitation dipole orientation of the SPE was only about 6°, suggesting that the absorption and the emission dipoles of this emitter were nearly parallel [27].

The effect of the NIR laser irradiation on the fluorescence of SPE was studied under a constant green laser with an average power of 45 μW. The signal-to-background ratio was 12.3:1. The inset of Fig. 2(a) is the scan image of the same SPE when we added the NIR pulsed laser beam with an average power of 33 mW. The image shows that the fluorescence from the SPE was completely suppressed, only leaving an unknown background with an intensity of 2.4 kcps that could be caused by other substrate impurities within the laser focus spot. When the NIR beam was added, the PL intensity dropped from 57.8 to 1.2 kcps. Meanwhile, the background also decreased from 4.7 to 2.4 kcps, leading to a signal-to-background ratio of 1:2. We measured the PL spectra of the SPE with two different NIR laser intensities as displayed in Fig. 2(b). When the average power of the NIR laser was about 0.55 mW, the PL spectrum showed the same spectral profile as the one excited by the green laser alone. When the NIR laser power was increased to 33 mW, the PL spectrum almost disappeared.

Regarding the polarization study, it was found that the polarization direction of the NIR laser affected the PL suppression efficiency. To demonstrate that, we did not choose the highest NIR power so the suppression was not expected to reach saturation. Instead, the NIR power was maintained at 0.55 mW to keep the suppression in the linear dynamic range. By tuning the polarization direction of the NIR laser with HWP2, the total PL intensity varied as shown in Fig. 2(c). The weakest suppression happened when the polarization direction of the NIR laser was almost parallel to that of the PL and the strongest suppression was observed at the perpendicular direction, indicating that the NIR laser interacted with a different energy level from those to produce PL.

Figure 2(d) displays the PL intensity variation as a function of the average power of both NIR (logarithmic scale) and green (linear scale) lasers. A smooth transition between these effects was observed in the same SPE with a nonmonotonic behavior as a function of both the green and NIR laser powers. The PL intensity increased with the green laser power until it was saturated. When the NIR laser was added, there was a gradual decrease in the PL intensity with the increase of the NIR laser power no matter whether the PL intensity was saturated or not. When the average power of the green laser was 45 μW and that of the NIR laser was 33 mW, corresponding to a peak power of 0.18 W and 132 W, respectively, the PL intensity was 57.8 kcps with only the green excitation and dropped to 1.2 kcps with the NIR laser suppression, resulting in the highest PL intensity suppression ratio of 97.9%.

We further investigated the suppression effect of the NIR laser on the PL emission lifetime by altering the delay time between the green laser and the NIR laser. The TCSPC was used here to record the PL decay by taking the laser pulse as the trigger signal. With the green laser excitation, the PL intensity decayed exponentially with a radiative lifetime of 2.1 ns as shown by the green curve in Fig. 3(a). This short emission lifetime enables the SPE to emit single photons at a high repetition rate. When the NIR laser was added, the PL emission lifetime varied dependent on the delay time between the green and the NIR laser. Figure 3(a) displays the evolution of the PL emission lifetime as a function of the delay time, revealing that the PL suppression reached the maximum when the two laser pulses overlapped each other at zero delay. The delay time in the experiment was limited to ±200 ps owing to the maximum length of the motorized translation stage. At negative delay time, i.e., the NIR laser was ahead of the green laser, the PL lifetime decay curve remained almost unchanged but the intensity decreased. However, at positive delay time, i.e., the green laser was ahead of the NIR laser, the shape of the PL lifetime decay curve underwent a significant change. The PL lifetime fell in half to be about 1 ns. The intensity decreased as well. To explain this change in the PL emission lifetime, a model involving four energy levels as shown in Fig. 3(b) is proposed. There is an excited state E and a ground state A, as well as two dark states (D1 and D2). At positive delay time, when the green pulse arrives before the NIR one, the emitter will be excited first to state E and the PL is switched off on the time-scale of the laser pulse since the emitter in the state E is excited to the dark state D2 by the subsequent NIR laser pulse. Different from the mechanism mentioned above, when the NIR pulse arrives earlier, the emitter is excited to the dark state D1 from the ground state A, leading to a lower probability of being excited to the state E, which makes the PL intensity decrease. Additionally, the shape of the PL lifetime decay curve at negative delays was the same as the original one, indicating that the radiation path of the emitter may be identical, and the dark state D1 is not excited. Due to the spectral cutting edges of the dichroic mirrors in the experimental setup, the spectrum shorter than 580 nm or longer than 960 nm could not be detected in the current experiment, making it difficult to determine whether the radiation from D1 or D2 is a non-radiative decay.

In order to investigate the NIR laser suppression response time, we complementally considered the photo-dynamics of the SPE. Since the delay line was not long enough to cover the whole suppression response time, we replaced the green pulsed laser by a continuous-wave one. A very fast intense suppression could be observed when the NIR laser illuminated,

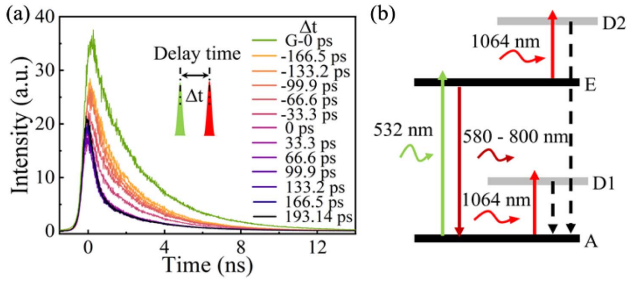

Fig. 3. (a) Evolution of the PL emission lifetime as a function of the delay between the green and the NIR laser pulses; (b) concept diagram of energy levels of an optical switch based on the SPE in 3C-SiC.

followed by slower relaxation to a steady state in the opposite direction proving the optical modulation is reversible. To eliminate the impact of the instrument itself, the original data were deconvoluted with the instrument response function (IRF) of our experimental setup, and the deconvoluted suppression response is shown in Fig. 4. The IRF was recorded as the TCSPC photon counting histogram of the green pulsed laser, using the laser pulse synchronization signal as the trigger and the APD output as the stop signal. Then the deconvoluted suppression response time was analyzed in two parts. Firstly, the falling edge of the suppression curve was fitted according to

$$I(t) = C\,\exp\left(-\frac{t}{t_0}\right) + C_0, \tag{2}$$

where C and C_0 are the fitting parameters and t_0 denotes the response time. The response time was 287.9 ± 5.7 ps, indicating that the suppression effect occurs within the range of pulse durations at a characteristic time much shorter than the instrumental response time. Then, the rising edge was fitted, showing a recovery time of 2.01 ± 0.05 ns, which may be the lifetime of dark state D2. The suppression response curve confirmed the energy levels involved in this optical switch.

In recent years, the optical switch based on the single NV center at room temperature is demonstrated under non-resonant continuous-wave illumination [8]. According to the latest report, the PL suppression in the NV center is attributed to the charge state conversion [28]. Multicolor illumination can raise the steady-state population of the negative charge state of the NV above 90% in specific regimes [29]. However, the optical switching response time of the NV center is about 100 ns, which was limited by the average PL lifetime of the NV center of about 12.3 ns [30]. Here, in our experiment, the measured PL lifetime of the SPE based on the defects in 3C-SiC was around 2.1 ns. Therefore, the emission process is much faster than that of NV centers in diamond. By exciting the SPE with a picosecond green pulsed laser and suppressing the PL with another picosecond NIR pulsed laser, the optical switching response time was measured to be as short as 287.9 ps, promising a high-speed optical switch at single-photon level. The high quality of the quantum emission and the prominent single-photon nature of the defects in 3C-SiC provide more potential applications in quantum technologies and hybrid optomechanics.

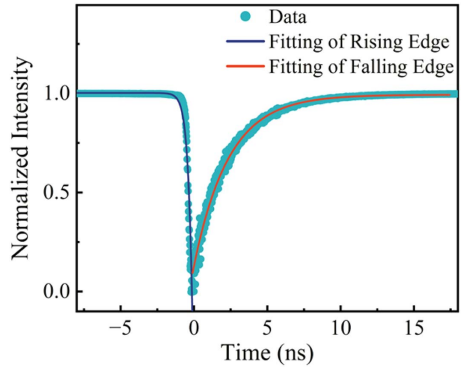

Fig. 4. Deconvolution of the PL response to the NIR laser pulse when pumped with a continuous-wave green laser, and fitting curves of rising and falling edges by the single exponential function. The inset is a schematic of the corresponding pulse sequence.

B. Application in Super-Resolution Imaging

The ultrafast reversible optical switch has significant applications in future quantum information processing devices, such as high-efficiency quantum memories [31], single-photon transistors [4], and single-photon gates [32]. Besides, as the NIR laser can suppress the PL of the SPE, it is possible to be employed in the super-resolution imaging using a similar strategy to STED. In our experiment, the NIR laser was used as the so-called STED beam. A vortex retarder was inserted in the NIR laser beam, which was used to generate the STED donut-shaped profile keeping the STED intensity nearly zero in the center of the focal spot and preserving the PL. The Gaussian-shaped green laser was the excitation beam superimposing on the doughnut-shaped NIR beam. The PL scan image of the SPE in $x \times y$ dimension pumped with only the pulsed green laser is illustrated in Fig. 5(a). Figure 5(b) shows the intensity plot along the dashed line in Fig. 5(a). A Gaussian fitting (red line) provides the spatial resolution of the microscope to be about 329.4 nm. By adding the doughnut-shaped NIR beam, a supper-resolution image beyond the diffraction limit was obtained as shown in Fig. 5(c). And a Gaussian fitting of the intensity profile in Fig. 5(d) gives a resolution of 96.4 nm when the NIR laser was at its maximum power of 33 mW, which is of about 3.4 times resolution improvement over that in Fig. 5(b). Due to imperfections of the vortex retarder, the non-symmetrical donut illumination resulted in an elliptical shape of the spot.

In the STED super-resolution microscope, the minimal resolving distance scales inversely with the square root of the saturation level (of STED), which is established as a law in the far-field optical microscopy resolution, extending Abbe's resolution equation [33]. The FWHM of the Gaussian fitting is approximated by a Taylor series to the second order as

$$\Delta r \approx 0.45\lambda/[n\,\sin\,\alpha \times (1+\varsigma)^{1/2}], \tag{3}$$

where ς is defined as the ratio of the maximum intensity I_{STED} to the excitation saturation laser intensity I_{sat}. And the latter is

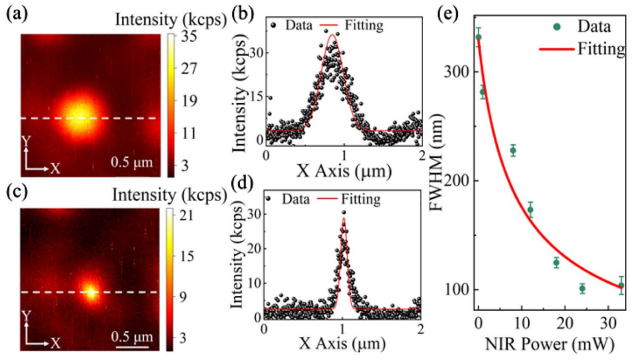

Fig. 5. (a) PL scan image in $x \times y$ dimension excited with only the green pulsed laser; (b) intensity profile along the dashed line in (a); (c) STED PL scan image in $x \times y$ dimension by adding the NIR laser donut depletion beam; (d) intensity profile along the dashed line in (c); (e) STED microscope resolution as a function of the NIR power. Error bars indicate the standard deviation in the Gaussian fitting.

defined by the PL lifetime of the sample and the absorption cross-section of the depletion beam ($I_{sat} = \hbar c/\lambda\tau\sigma$). λ and $n \sin \alpha$ represent the wavelength of the STED beam and the numerical aperture of the objective microscope lens, respectively [34]. Figure 5(e) indicates the enhancement of the resolution with the increase of the NIR beam power. The red line is the fitting according to Eq. (3). In our experiment, at the maximum NIR power of 33 mW, the highest resolution of about 96.4 nm was obtained, very close to the limit value. Theoretically, the spatial resolution can be improved unlimitedly by increasing the depletion laser power. The gain in the resolution is moderate since the depletion laser intensity at the doughnut beam center is not ideally zero. In the meantime, increasing the depletion laser power will decrease the contrast of the image and the symmetry of the spot shape.

4. CONCLUSION

It is demonstrated that when the high-power picosecond NIR pulsed laser and the green pulsed laser were simultaneously illuminated on the room-temperature SPE in bulk 3C-SiC crystals, reversible and ultrafast PL suppression was achieved with a highest efficiency of 97.9%. This effect was maximal when the NIR pulse and the green pulse arrived simultaneously onto the SPE. We proposed that the observed PL suppression under the NIR pulsed illumination resulted from the presence of dark bands that can be optically activated with the NIR laser. The modulation has an ultrafast suppressive response time as short as 287.9 ± 5.7 ps, supporting the development of an ultrafast optical switch. Our experiment has implemented the nonlinear effects at the single-photon level, which is highly desirable as it can drive the power consumption of all-optical switches, optical modulators, and optical transistors to their fundamental limit [35]. Furthermore, it can offer unique applications for optical quantum control and new paradigms for optical computing, optical communications, and metrology [36,37].

Funding. National Key Research and Development Program of China (2021YFA1201503); National Natural Science Foundation of China (12274137).

Acknowledgment. The authors acknowledge Professor Sanjun Zhang and Professor Jinquan Chen for their insightful discussions on the theoretical model.

Disclosures. The authors declare no conflicts of interest.

Data Availability. Data underlying the results presented in this paper are not publicly available at this time but may be obtained from the authors upon reasonable request.

REFERENCES

1. J. Clark and G. Lanzani, "Organic photonics for communications," Nat. Photonics **4**, 438–446 (2010).
2. D. Thomson, A. Zilkie, J. E. Bowers, *et al.*, "Roadmap on silicon photonics," J. Opt. **18**, 073003 (2016).
3. B. Hacker, S. Welte, G. Rempe, *et al.*, "A photon-photon quantum gate based on a single atom in an optical resonator," Nature **536**, 193–196 (2016).
4. J. Hwang, M. Pototschnig, R. Lettow, *et al.*, "A single-molecule optical transistor," Nature **460**, 76–80 (2009).
5. D. E. Chang, A. S. Sorensen, E. A. Demler, *et al.*, "A single-photon transistor using nanoscale surface plasmons," Nat. Phys. **3**, 807–812 (2007).
6. A. Micheli, A. J. Daley, D. Jaksch, *et al.*, "Single atom transistor in a 1D optical lattice," Phys. Rev. Lett. **93**, 140408 (2004).
7. F. He and K.-D. Zhu, "Single molecule photonic transistor and router through plasmonic nanocavity," Appl. Phys. B **129**, 65 (2023).
8. M. Geiselmann, R. Marty, F. Javier García de Abajo, *et al.*, "Fast optical modulation of the fluorescence from a single nitrogen-vacancy centre," Nat. Phys. **9**, 785–789 (2013).
9. N. Bar-Gill, L. Pham, A. Jarmola, *et al.*, "Solid-state electronic spin coherence time approaching one second," Nat. Commun. **4**, 1743 (2013).
10. D. Farfurnik, A. Jarmola, L. M. Pham, *et al.*, "Optimizing a dynamical decoupling protocol for solid-state electronic spin ensembles in diamond," Phys. Rev. B **92**, 060301 (2015).
11. J. Wang, W. Zhang, J. Zhang, *et al.*, "Coherence times of precise depth controlled NV centers in diamond," Nanoscale **8**, 5780–5785 (2016).
12. O. Chen, J. Zhao, V. P. Chauhan, *et al.*, "Compact high-quality CdSe-CdS core-shell nanocrystals with narrow emission linewidths and suppressed blinking," Nat. Mater. **12**, 445–451 (2013).
13. W. F. Koehl, B. B. Buckley, F. J. Heremans, *et al.*, "Room temperature coherent control of defect spin qubits in silicon carbide," Nature **479**, 84–87 (2011).
14. H. Seo, A. L. Falk, P. V. Klimov, *et al.*, "Quantum decoherence dynamics of divacancy spins in silicon carbide," Nat. Commun. **7**, 12935 (2016).
15. A. Bourassa, C. P. Anderson, K. C. Miao, *et al.*, "Entanglement and control of single quantum memories in isotopically engineered silicon carbide," J. Phys. Chem. Lett. **11**, 1675–1681 (2020).
16. M. Widmann, S. Y. Lee, T. Rendler, *et al.*, "Coherent control of single spins in silicon carbide at room temperature," Nat. Mater. **14**, 164–168 (2014).
17. C. P. Anderson, A. Bourassa, K. C. Miao, *et al.*, "Electrical and optical control of single spins integrated in scalable semiconductor devices," Science **366**, 1225–1230 (2019).
18. L. Li, X. Guo, P. B. Ding, *et al.*, "Ultrafast all-optical switching in the visible spectrum with 6H silicon carbide," ACS Photonics **8**, 2940–2946 (2021).
19. S. Castelletto, M. Barbiero, M. Charnley, *et al.*, "Imaging with nanometer resolution using optically active defects in silicon carbide," Phys. Rev. Appl. **14**, 034021 (2020).
20. J. Y. Zhou, Q. Li, Z. H. Hao, *et al.*, "Plasmonic-enhanced bright single spin defects in silicon carbide membranes," Nano Lett. **23**, 4334–4343 (2023).
21. T. Nakanuma, K. Tahara, K. Kutsuki, *et al.*, "Control on the density and optical properties of color centers at SiO_2/SiC interfaces by oxidation and annealing," Appl. Phys. Lett. **123**, 102102 (2023).
22. J. F. Wang, Q. Li, F. F. Yan, *et al.*, "On-demand generation of single silicon vacancy defects in silicon carbide," ACS Photonics **6**, 1736–1743 (2019).
23. J. F. Wang, Z. H. Liu, F. F. Yan, *et al.*, "Experimental optical properties of single nitrogen vacancy centers in silicon carbide at room temperature," ACS Photonics **7**, 1611–1616 (2020).
24. A. Lohrmann, S. Castelletto, J. R. Klein, *et al.*, "Activation and control of visible single defects in 4H-, 6H-, and 3C-SiC by oxidation," Appl. Phys. Lett. **108**, 021107 (2016).
25. M. T. He, Z. P. Ju, Y. X. Xue, *et al.*, "Bright single-photon emitters in cubic silicon carbide," IEEE J. Sel. Top. Quantum Electron. **30**, 0100106 (2023).
26. E. Neu, M. Fischer, S. Gsell, *et al.*, "Fluorescence and polarization spectroscopy of single silicon vacancy centers in heteroepitaxial nanodiamonds on iridium," Phys. Rev. B **84**, 5211–5220 (2011).
27. N. R. Jungwirth, B. Calderon, Y. Ji, *et al.*, "Temperature dependence of wavelength selectable zero-phonon emission from single defects in hexagonal boron nitride," Nano Lett. **16**, 6052–6057 (2016).

28. P. Qian, Y. P. Zhai, J. Hu, *et al.*, "Multicolor-illuminated charge-state dynamics of the nitrogen-vacancy center in diamond," Phys. Rev. A **106**, 033506 (2023).
29. D. A. Hopper, R. R. Grote, A. L. Exarhos, *et al.*, "Near-infrared-assisted charge control and spin readout of the nitrogen-vacancy center in diamond," Phys. Rev. B **94**, 241201 (2016).
30. R. Nelz, J. Görlitz, D. Herrmann, *et al.*, "Toward wafer-scale diamond nano- and quantum technologies," APL Materials **7**, 011108 (2019).
31. M. Albert, A. Dantan, and M. Drewsen, "Cavity electromagnetically induced transparency and all-optical switching using ion coulomb crystals," Nat. Photonics **5**, 633–636 (2011).
32. X. Su, J. S. Tang, and K. Y. Xia, "Nonlinear dissipation-induced photon blockade," Phys. Rev. A **106**, 063707 (2022).
33. A. V. Zasedatelev, A. V. Baranikov, D. Sannikov, *et al.*, "Single-photon nonlinearity at room temperature," Nature **597**, 493–497 (2021).
34. V. Westphal and S. W. Hell, "Nanoscale resolution in the focal plane of an optical microscope," Phys. Rev. Lett. **94**, 143903 (2005).
35. S. T. Hell, "Toward fluorescence nanoscopy," Nat. Biotechnol. **21**, 1347–1355 (2003).
36. I. A. Walmsley, "Quantum optics: science and technology in a new light," Science **348**, 525–530 (2015).
37. D. E. Chang, V. Vuletić, and M. D. Lukin, "Quantum nonlinear optics-photon by photon," Nat. Photonics **8**, 685–694 (2014).